L-Edge X-ray Absorption and X-ray Magnetic Circular Dichroism of Oxygen-Bridged Dinuclear Iron Complexes

G. Peng,[†] J. van Elp,[‡] H. Jang,[§] L. Que, Jr.,[§] W. H. Armstrong,[||] and S. P. Cramer*,[†,‡]

Contribution from the Department of Applied Science, University of California, Davis, California 95616, Energy and Environment Division, Lawrence Berkeley Laboratory, Berkeley, California 94720, Department of Chemistry, University of Minnesota, Minneapolis, Minnesota 55455, and Department of Chemistry, Boston College, Boston, Massachusetts 02169

Received September 12, 1994[⊗]

Abstract: Iron L-edge X-ray absorption and X-ray magnetic circular dichroism (XMCD) spectroscopy have been used to study the electronic structure of dinuclear iron–oxo complexes with different types of magnetic and electronic interactions between the iron sites. Trapped-valence systems exhibit L-edges with clear multiplet structure. The L-edges of trapped-valence $Fe^{II}Fe^{III}$ complexes such as $[Fe^{III,II}_2(salmp)_2]^-$ and $[Fe_2^{III,II}(bpmp)(\mu\text{-}O_2CC_2H_5)_2]^{2-}$ can be interpreted as the sum of distinct Fe(II) and Fe(III) component spectra. Furthermore, an atomic multiplet theory including adjustable ligand field splittings can successfully simulate the Fe(II) and Fe(III) X-ray absorption. Reasonable ligand field parameters are obtained by optimizing the correspondence between calculated and experimental spectra. The XMCD for the $[Fe_2^{III,II}(bpmp)(\mu\text{-}O_2CC_2H_5)_2]^{2-}$ complex is also reported; it exhibits an interesting magnetic field dependence that reflects the weak magnetic coupling between Fe(II) and Fe(III) ions. In contrast with the trapped-valence complex spectra, the L-edge spectrum for the electronically delocalized complex, $[Fe_2(Me_3tacn)_2(\mu\text{-}OH)_3](BPh_4)_2\cdot 2MeOH$, exhibits a broad L-edge spectrum with poorly resolved multiplet structure. L-edge spectroscopy is capable of characterizing electron delocalization on a very fast (femtosecond) time scale, while XMCD is an alternative technique for characterizing exchange interactions.

Introduction

Mixed-valence iron complexes[1] are important as magnetic materials, in geochemistry, in corrosion, and in metalloprotein clusters.[2] Commonly used techniques for characterizing the electronic structure and magnetic interactions include electronic spectroscopy, magnetic resonance methods, polarized neutron diffraction, K-edge X-ray absorption (XAS), and Mössbauer spectroscopy.[3] Recent improvements in soft X-ray beam line optics,[4] fluorescence detectors,[5] and interpretation methods[6] have made Fe L-edge X-ray absorption spectroscopy a viable technique which is complementary to these other methods. The 2p → 3d transitions at L-edges are strong and dipole-allowed (as opposed to the weak forbidden 1s → 3d transitions at K-edges). L-edges also have smaller natural line widths and the possibility of strong magnetic circular dichroism.[7]

The final state for a first transition metal L-edge transition has a 2p core hole. Coulomb and exchange interactions between this core hole and the 3d valence electrons make L-edge XAS sensitive to the number and configuration of 3d electrons, hence to the spin state and oxidation state.[8,9] The small lifetime broadening of the 2p core hole results in sharp multiplet structure at the $L_{2,3}$-edges, which often makes an unambiguous theoretical interpretation possible. L-edge XAS has recently been used to study the electronic structure and symmetry of biologically relevant Mn and Ni complexes[10,11] as well as several metalloprotein redox centers or active sites, including the Fe in *Pyrococcus furiosus* rubredoxin,[12] Cu in plastocyanin,[13] and Ni in substituted rubredoxin[11] and hydrogenase.[14] L-edges can also exhibit intense X-ray magnetic circular dichroism (XMCD), and strong effects have recently been demonstrated on several biological systems, such as the Fe center in *P. furiosus* rubredoxin[15] and in the *Clostridium pasteurianum* 2Fe–2S protein.[16]

[†] University of California, Davis.
[‡] Lawrence Berkeley Laboratory.
[§] University of Minnesota.
[||] Boston College.
[⊗] Abstract published in *Advance ACS Abstracts*, February 1, 1995.

(1) Robin, M. D.; Day, P. *Adv. Inorg. Chem. Radiochem.* **1967**, *10*, 247.
(2) (a) Que, L., Jr.; Scarrow, R. C. In *Metal Clusters in Proteins*; Que, L., Jr., Ed.: ACS Symposium Series 372; American Chemical Society: Washington, DC, 1988; pp 159–178. (b) Lippard, S. J. *Angew. Chem., Int. Ed. Engl.* **1988**, *27*, 344.
(3) Reed, C. A.; Orosz, R. D. In *Research Frontiers in Magnetochemistry*; O'Connor, C. J., Ed.; World Scientific Publishing Co.: 1993, p 351.
(4) (a) Chen, C. T.; Sette, F. *Rev. Sci. Instr.* **1989**, *60*, 1616–1621. (b) Chen, C. T. *Rev. Sci. Instrum.* **1992**, *63*, 1229–1233. (c) Chen, C. T.; Sette, F.; Smith, N. V. *Appl. Opt.* **1990**, *29*, 4535–4536.
(5) Cramer, S. P.; Chen, J.; George, S. J.; van Elp, J.; Moore, J.; Tench, O.; Colaresi, J.; Yocum, M.; Mullins, O. C.; Chen, C. T. *Nucl. Instrum. Methods Phys. Res., Sect. A* **1992**, *319*, 285.
(6) de Groot, F. M. F.; Fuggle, J. C.; Thole, B. T.; Sawatzky, G. A. *Phys. Rev. B* **1990**, *42*, 5459.
(7) van der Laan, G.; Thole, B. T. *Phys. Rev. B* **1990**, *42*, 6670–6674.
(8) van der Laan, G.; Thole, B. T.; Sawatzky, G. A.; Verdaguer, M. *Phys. Rev. B* **1988**, *37*, 6587–6589.
(9) van der Laan, G.; Kirkman, I. W. *J. Phys.: Condens. Matter* **1992**, *4*, 4189.
(10) Cramer, S. P.; de Groot, F. M. F.; Ma, Y.; Chen, C. T.; Sette, F.; Kipke, C. A.; Eichhorn, D. M.; Chan, M. K.; Armstrong, W. H.; Libby, E.; Christou, C.; Brooker, S.; McKee, V.; Mullins, O. C.; Fuggle, J. C. *J. Am. Chem. Soc.* **1991**, *113*, 7937.
(11) van Elp, J.; Peng, G.; Searle, B. G.; Mitra-Kirtley, S.; Huang, Y.-H.; Johnson, M. K.; Zhou, Z. H.; Adams, M. W. W.; Maroney, M. J.; Cramer, S. P. *J. Am. Chem. Soc.* **1994**, *116*, 1918.
(12) George, S. J.; van Elp, J.; Chen, J.; Park, J.-B.; Adams, M. W. W.; Searle, B. G.; de Groot, F. M. F.; Fuggle, J. C.; Cramer, S. P. *J. Am. Chem. Soc.* **1992**, *114*, 4426.
(13) George, S. J.; Lowery, M. D.; Solomon, E. I.; Cramer, S. P. *J. Am. Chem. Soc.* **1993**, *115*, 2968.
(14) van Elp, J.; Peng, G.; Zhou, Z. H.; Adams, M. W. W.; Baidya, N.; Mascharak, P. K.; Cramer, S. P. *Inorg. Chem.*, in press.

0002-7863/95/1517-2515$09.00/0

Scheme 1. General Structures for Some of the Fe Complexes Examined in this Paper

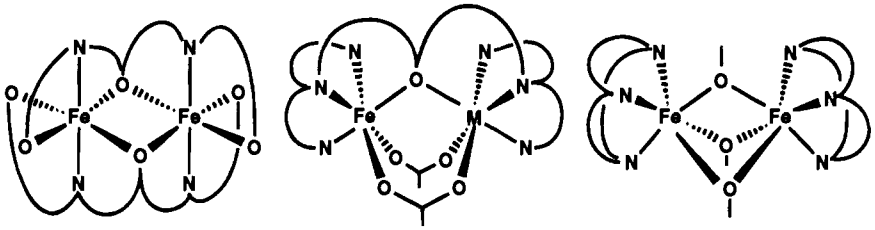

$[Fe_2(salmp)_2]^{0,1-,2-}$ $[FeM(bpmp)(\mu\text{-}OPr)_2]^{n+}$ n=2, M=Fe, Zn, Ga; n=1, M=Fe $[Fe_2(Me_3tacn)_2(\mu\text{-}OH)_3]^{2+}$

In this paper, three types of oxygen-bridged binuclear Fe complex systems, $[Fe_2(salmp)_2]^{0,-,2-}$, $[FeM(bpmp)(\mu\text{-}O_2CC_2H_5)_2]^{n+}$, and $[Fe_2(Me_3tacn)_2(\mu\text{-}OH)_3]^{2+}$, are studied by a combination of L-edge and XMCD spectroscopy.[17] These systems have similar coordination environments, involving oxygen and nitrogen ligands in a distorted octahedral symmetry. However, the complexes have very different degrees of electronic delocalization and types of magnetic exchange interactions between the two iron sites.

The $[Fe_2(salmp)_2]^{0,-,2-}$ complexes have $[Fe-O_4N_2]$ coordination, as shown in Scheme 1.[18] The mixed-valence form $[Fe_2(salmp)_2]^-$ exhibits ferromagnetic coupling between the Fe ions to yield an $S = {}^9/_2$ ground state, and on the basis of UV–vis spectroscopy, it belongs to class II in the Robin–Day classification scheme.[1] The $[FeM(bpmp)(\mu\text{-}O_2CC_2H_5)_2]^{n+}$ complexes, where M can be Fe,[19] Ga, or Zn,[20] have distorted octahedral symmetry with $[Fe-O_3N_3]$ coordination (Scheme 1). The mixed-valence form is again class II, but the coupling between Fe ions is antiferromagnetic to yield an $S = {}^1/_2$ ground state. Finally, the electronically delocalized mixed-valence complex $[Fe_2(Me_3tacn)_2(\mu\text{-}OH)_3]^{2+}$ also has $[Fe-O_3N_3]$ coordination, but belongs to class III in the Robin–Day scheme.[21] Two mononuclear iron complexes with $[Fe-N_6]$ coordination, $[Fe(tppb)_2]$[22] and $[Fe(HB(pz)_3)_2][ClO_4]$,[23] were also studied to probe the effects of the ligand field and spin state on L-edge spectra.

Experimental Section

Preparation of Compounds. $[Et_4N]_2[Fe^{III}_2(salmp)_2]$, $[Et_4N][Fe^{III,II}_2(salmp)_2]$, $[Fe^{II,II}_2(salmp)_2]$, and $[Fe^{III,II}_2(Me_3tacn)_2(OH)_3][BPh_4]_2$·2MeOH were prepared in the Cramer lab by the published methods.[18,21] $[Fe^{III}Zn^{II}(bpmp)(\mu\text{-}O_2CC_2H_5)_2][BPh_4]_2$, $[Fe^{III,II}_2(bpmp)(\mu\text{-}O_2CC_2H_5)_2][BPh_4]_2$, $[Fe^{II}Ga^{III}(bpmp)(\mu\text{-}O_2CC_2H_5)_2][BPh_4]_2$, and $[Fe^{II,II}_2(bpmp)(\mu\text{-}O_2CC_2H_5)_2][BPh_4]$ were prepared in the Que lab.[19,20] $[Fe(tppb)_2]$[22] and $[Fe(HBpz_3)_2][ClO_4]$[23] were prepared in the Armstrong lab. The XMCD samples were obtained by diluting the mixed-valence complexes with $[Ph_4N][BPh_4]$ (from Aldrich) to 1.5 wt %. The dilution process used very fast removal of the solvent (CH_3CN) to avoid fractional recrystallization of the mixed-valence complex.

X-ray Data Collection. The X-ray absorption spectra were recorded at AT&T beam line U4B at the National Synchrontron Light Source[4] using total electron yield detection. Finely powdered samples were placed on double adhesive tape and transferred anaerobically to a helium cryostat cold finger in the main chamber. The energy resolution was set to about 160 meV using 20 μm entrance and exit slits. All of the reported spectra were taken at low temperatures (~10 K) and under a vacuum of at least 2×10^{-9} mbar. No significant changes in absorption spectra for $[Fe_2(salmp)_2]^-$ or $[FeZn(bpmp)(\mu\text{-}O_2CC_2H_5))_2]^{2+}$ were observed in the temperature range 10–293 K. The samples were also checked for surface degradation by comparison of the fluorescence yield and total electron yield signals, and no evidence for surface degradation was found. The X-ray energy scale was calibrated using the peak positions of the total electron yield spectrum of $K_4Fe(CN)_6$ (L_3 peaks at 710.35 and 712.05 eV). For comparison with the theoretical calculations, a base-line curve was subtracted by using a polynomial function fitted to the data in front of the L_3-edge region and beyond the L_2-edge region.

The XMCD experiments used beam line U4B in the double-headed configuration.[4] The degree of circular polarization was set to around 80% and the energy resolution was set to 625 meV, by adjusting slit positions and widths. Details about the XMCD apparatus have been published.[15,24] The XMCD spectra were internally calibrated by doping the sample with Cs(acac) (from Aldrich), which has an M_5-edge at 735.0 eV. The 6 T spectrum represents the average of eight scans, each scan with 3 s counting per data point. For these scans there were about 130 counts/s for the edge jump and about 60 counts/s for background. The 1 T spectrum used 12 scans, again with 3 s counting per data point. For these scans there were about 200 counts/s for the edge jump and about 50 counts/s for background. The XMCD spectra were normalized to the background in regions of 10 eV before the L_3-edge and 10 eV after the L_2-edge.

Atomic Multiplet Calculations. Ligand field atomic multiplet calculations were performed for divalent and trivalent Fe using published methods.[6,9] The X-ray transitions for $2p^63d^5 \rightarrow 2p^53d^6$ for Fe^{3+} and $2p^63d^6 \rightarrow 2p^53d^7$ for Fe^{2+}. In O_h symmetry the 3d orbitals are split into e_g (x^2-y^2, $3z^2-r^2$) and t_{2g} (xy, yz, xz) orbitals with an energy difference of $10Dq$. In lowering the symmetry to D_{4h} or D_{3d}, the orbitals are further split, and the splittings are described by the ligand field parameters Ds and Dt in D_{4h} symmetry and D_0 in D_{3d} symmetry. These ligand field parameters were adjusted to yield a good match between calculated and experimental spectra. The *ab initio* Hartree–Fock values of the Slater integrals and spin–orbit couplings (ξ_{2p} and ξ_{3d}) were used as tabulated. Charge transfer effects are taken into account by a reduction of the Slater integrals in the calculation. The spectra are broadened with a Lorentzian with width 2Γ eV (FWHM) and convoluted with a Gaussian with width σ eV to describe the lifetime and instrumental broadening, respectively.

Results and Discussion

The L-edge spectra for the $[Fe_2(salmp)_2]^{0,-,2-}$ system are shown in Figure 1. The spectra are split into two regions by

(15) van Elp, J.; George, S. J.; Chen, J.; Peng, G.; Chen, C. T.; Tjeng, L. H.; Meigs, G.; Lin, H.-J.; Zhou, Z. H.; Adams, M. W. W.; Searle, B. G.; Cramer, S. P. *Proc. Natl. Acad. U.S.A.* **1993**, *90*, 9664.

(16) van Elp, J.; Peng, G.; Cramer, S. P. Unpublished results.

(17) Abbreviations: bpmp, 2,6-bis[bis(2-pyridylmethyl)aminomethyl]-4-methylphenolate(1−); Me_3tacn, 1,4,7-trimethyl-1,4,7-triazacyclononane; salmp, bis(salicylideneamino)-2-methylphenolate(3−); tppb, hydrotris(3-phenylpyrazol-1-yl)borate; $HB(pz)_3$, β-hydrotris(pyrazol-1-yl)borate; Phen, *o*-phenanthroline; acac, acetylactone.

(18) Snyder, B. S.; Patterson, G. S.; Abrahamson, A. J.; Holm, R. H. *J. Am. Chem. Soc.* **1989**, *111*, 5214.

(19) Borovik, A. S.; Que, L., Jr. *J. Am. Chem. Soc.* **1988**, *110*, 2345.

(20) Borovik, A. S.; Que, L., Jr.; Papaefthymiou, V.; Münck, E.; Taylor, L. F.; Anderson, O. P. *J. Am. Chem. Soc.* **1988**, *110*, 1986.

(21) Drueker, S.; Chaudhuri, P.; Pohl, K.; Wieghardt, K.; Bill, E.; Sawaryn, A.; Trautwein, A. X.; Winkler, H.; Gurman, S. J. *J. Chem. Soc., Chem. Commun.* **1989**, 59.

(22) Eichhorn, D. M.; Armstrong, W. H. *Inorg. Chem.* **1990**, *29*, 3607.

(23) Trofimenko, S. *J. Am. Chem. Soc.* **1967**, *89*, 3170.

(24) George, S. J.; van Elp, J.; Chen, J.; Peng, G.; Mitra-Kirtley, S.; Mullins, O. C.; Cramer, S. P. In *Synchrotron Radiation in Biosciences*; Chance, B., Ed.; Oxford University Press: New York, 1994.

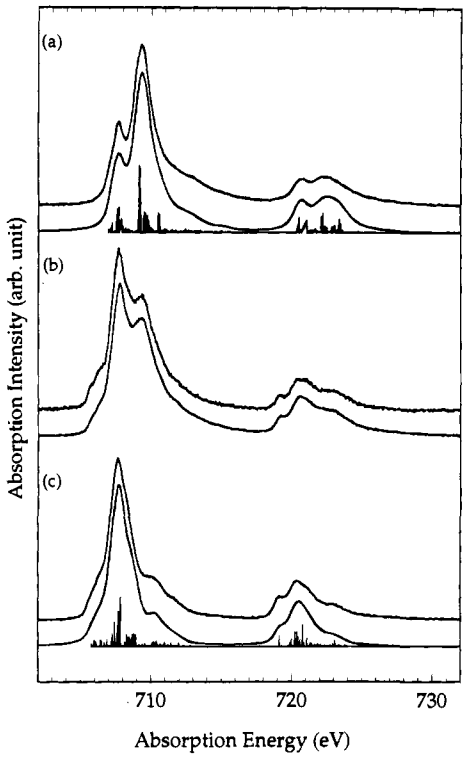

Figure 1. (a) Experimental L-edge spectrum (top) of $[Fe_2^{III,III}(salmp)_2]$ together with the theoretical calculation (bottom). (b) Experimental L-edge spectrum (top) of $[Fe_2^{III,II}(salmp)_2]^-$ together with a summation, based on the experimental spectra for Fe(III)−Fe(III) and Fe(II)−Fe(II) (bottom). (c) Experimental L-edge spectrum (top) for $[Fe_2^{II,II}(salmp)_2]^{2-}$ together with a theoretical calculation (bottom). The stick diagrams show the strengths of individual transitions before broadening.

the 2p spin−orbit interaction. The L_3-edge ($2p_{3/2}$ hole) is found at about 709 eV and the L_2-edge ($2p_{1/2}$ hole) around 722 eV. Each complex contains ferromagnetically coupled iron pairs: Fe(III)−Fe(III), Fe(III)−Fe(II), and Fe(II)−Fe(II), with S_{total} = 5, $^9/_2$, and 4 for the ground states, respectively. In the mixed-valence dimer, the two trapped-valence irons are separated by 3.08 Å and coupled with J = 8.6 cm^{-1},[25] where J is the intramolecular exchange interaction, $\mathbf{H} = -2J\mathbf{S}_1\cdot\mathbf{S}_2$. For the Fe(III)−Fe(III) complex (Figure 1a), there are two peaks in the L_3 region, a smaller one at 707.7 eV and an overall maximum at 709.3 eV. A less-resolved double-peaked structure occurs at the L_2-edge. Similar spectra are also found in Fe_2O_3[26] and $LaFeO_3$;[27] this is a characteristic pattern for high-spin Fe(III) (d^5) in octahedral symmetry. A calculation with a 10Dq value of 1.5 eV reproduces the experimental spectrum well. This value is similar to previous results of 1.65 eV for Fe_2O_3[26] and 1.8 eV for $LaFeO_3$[27] and the 10Dq = 1.7 eV found for Fe^{3+} in aqueous solution by optical spectroscopy.[28]

The optimum 10Dq value is mainly determined by the splitting between the two peaks in the L_3 region. Calculations with distorted octahedral symmetry show that the d^5 configuration, atomic ^{6}S ground state or $^6A_{1g}$ state in O_h symmetry, is not sensitive to either D_{3d} or D_{4h} distortions; this is because the ground state has a half-filled d-shell. The additional parameters used for the simulations are provided as supplementary material.

The spectrum of the Fe(II)−Fe(II) salmp complex (Figure 1c) has an overall maximum L_3 at 707.7 eV with shoulders on both high- and low-energy sides. The 1.6 eV shift in peak position, as compared to the fully oxidized complex, is similar to that found for ionic Mn complexes.[10] The L_2 region is a triplet centered at 720.4 eV. Both regions of the spectrum can be reproduced by a calculation with a 10Dq of 0.9 eV, including a D_{3d} distortion with D_0 = 0.1 eV. The D_{3d} distortion is especially important for improving agreement at the high-energy shoulder of the L_3-edge and low-energy side of the L_2 peak. The D_0 parameter splits the t_{2g} band by approximately $3D_0$ into a_1 and e symmetry components.[29] Although the salmp ligand creates an environment which is structurally described as distorted D_{4h} symmetry, with two axial nitrogen ligands and four equatorial oxygens, simulation of the spectra shows that the electronic structure of this compound can be better described with a D_{3d} distortion. The distortion from O_h symmetry combined with spin−orbit coupling creates a zero-field splitting pattern with m_s = 0 as the lowest state with a calculated D of 1.5 meV (12 cm^{-1}).

The spectrum for the Fe(II)−Fe(III) mixed-valence salmp complex (Figure 1b) has two resolved L_3 region peaks and a triplet L_2 region. All of these spectral features are reproduced by a linear combination of the Fe(II)−Fe(II) and Fe(III)−Fe(III) spectra (Figure 1b). This indicates that the Fe(II) and Fe(III) sites can be treated as electronically isolated species with regard to X-ray absorption. This conclusion is consistent with Mössbauer measurements[25] which also found trapped-valence Fe sites. We note that Mössbauer spectroscopy has a much larger time scale of 10^{-7} s, as compared to the X-ray absorption time scale of about 10^{-15} s.

The spectra for $[FeM(bpmp)(\mu\text{-}O_2CC_2H_5)_2]^{2+,+}$ with M = Fe and Zn are shown in Figure 2. The Zn-substituted complex was employed in order to form a complete set of Fe oxidation states because the Fe(III)−Fe(III) complex is not available. The spectrum for the Fe(III)−Zn bpmp complex is quite similar to the $[Fe^{III}_2(salmp)_2]$ spectrum, with a small peak at lower energy in the L_3 region, followed by an overall maximum that tails to the higher energy side. A slightly lower 10Dq value of 1.6 eV gave the best simulation.

The spectrum for $[Fe^{II}_2(bpmp)(\mu\text{-}O_2CC_2H_5)_2]^+$ (Figure 2c) is somewhat different from the corresponding $[Fe^{II}_2(salmp)_2]^{2-}$ spectrum. The L_3 features that were simply high-energy shoulders in the salmp spectrum are not resolved peaks in the bpmp spectrum. The $[Fe^{II}Ga(bpmp)(\mu\text{-}O_2CC_2H_5)_2]^{2+}$ samples give nearly identical spectra (not shown). This is consistent with a localized electron description for the $2p \rightarrow 3d$ transitions. A similar spectrum without the extra high energy peak is also observed for $[Fe^{II}(phen)_2(NCS)_2]$,[30] in which the Fe has an approximately O_h symmetry. In the simulations, a larger 10Dq value (1.1 eV) reproduces the peak positions quite well, but the intensity of the peak at 710.2 eV is low. Some of this intensity may come from satellite structure for a $2p^53d^8\underline{L}$ ($\underline{L}$ refers to a ligand hole) final state, because a similar structure is also observed beyond the L_2-edge.

The Fe−Fe distance in the mixed-valence complex is 3.365 Å, and the two irons are antiferromagnetically coupled to yield an $S_{total} = {}^1/_2$ ground state with $J = -2.5$ cm^{-1}.[19] The spectrum for the mixed-valence Fe(III)−Fe(II) bpmp complex has two strong peaks in the L_3 region split by 2.0 eV and two weak peaks in a broader L_2 region (Figure 2b). As with the salmp spectrum, the mixed-valence bpmp spectrum can be simulated

(25) Surerus, K. K.; Münck, E.; Snyder, B. S.; Holm, R. H. *J. Am. Chem. Soc.* **1989**, *111*, 5501.
(26) Kuiper, P.; Searle, B. G.; Rudolf, P.; Tjeng, L. H.; Chen, C. T. *Phys. Rev. Lett.* **1993**, *70*, 1549.
(27) Abbate, M.; de Groot, F. M. F.; Fuggle, J. C.; Fujimori, A.; Strebel, O.; Lopez, F.; Domke, M.; Kaindl, G.; Sawatzky, G. A.; Takano, M.; Takeda, Y.; Eisaki, H.; Uchida, S. *Phys. Rev. B* **1992**, *46*, 4511.
(28) Jorgensen, C. K. *Absorption Spectra and Chemical Bonding in Complexes*; Pergamon: Oxford, 1962.
(29) Ballhausen, C. J. *Introduction to Ligand Field Theory*; McGraw-Hill: New York, 1962.
(30) dit Moulin, C. C.; Rudolf, P.; Flank, A.-M.; Chen, C. T. *J. Phys. Chem.* **1992**, *96*, 6196.

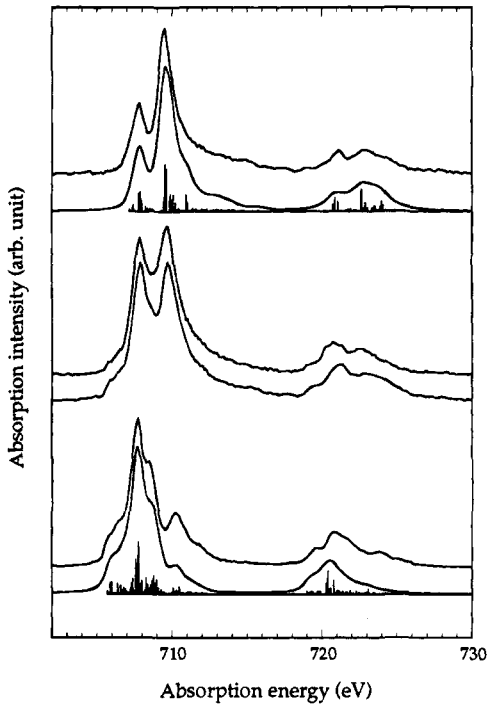

Figure 2. (a) Experimental L-edge spectrum (top) of $[Fe^{III}Zn(bpmp)(\mu\text{-}O_2CC_2H_5)_2][BPh_4]_2$ together with the theoretical calculation (bottom). (b) Experimental L-edge spectrum (top) of $[Fe_2^{III,II}(bpmp)(\mu\text{-}O_2CC_2H_5)_2][BPh_4]_2$ together with a summation, based on the experimental spectra for Fe(III)−Zn and Fe(II)−Fe(II) (bottom). (c) Experimental L-edge spectra (top) for $[Fe_2^{II,II}(bpmp)(\mu\text{-}O_2CC_2H_5)_2][BPh_4]$ together with a theoretical calculation (bottom). The stick diagrams show the strengths of individual transitions before broadening.

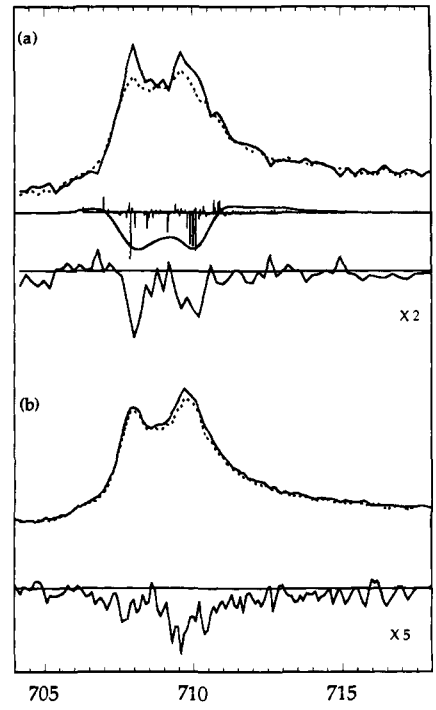

Figure 3. XMCD spectra for $[Fe_2^{III,II}(bpmp)(\mu\text{-}O_2CC_2H_5)_2][BPh_4]_2$ in different magnetic fields. (a) XMCD spectrum at 6 T: top, excitation spectra with left (···) and right (—) circular polarization; middle, the sum of calculated XMCD spectra for ferrous and ferric ions (the stick diagrams show the strengths of individual transitions before broadening); bottom, experimental XMCD spectrum (the maximum observed XMCD effect at 6 T was 14%). (b) XMCD spectrum at 1 T: top, excitation spectra with left (···) and right (—) circular polarization; bottom, experimental XMCD spectrum (maximum observed XMCD effect at 1 T was 4%).

by summing the experimental spectra of reduced and oxidized forms, in this case the spectra for the Fe(III)−Zn and Fe(II)−Fe(II) complexes. This result is again consistent with the Mössbauer spectra, where the high-spin Fe(III) and Fe(II) yield two quadruple doublets of equal intensity.[19]

Additional information about the electronic structure and the strength of exchange interactions in mixed-valence systems can be obtained from the relatively new technique of X-ray magnetic circular dichroism (XMCD). Theoretical calculations predict a negative XMCD effect at the L_3-edge (when defined as $\mu_L - \mu_R$) where the magnetic moment of a transition metal or rare earth is aligned with the magnetic field.[31] For antiferromagnetically coupled systems, the XMCD for the ions with majority spin orientation will be negative, while the minority spin ions will have positive XMCD signals. Chen and co-workers have used this effect in experiments on the $Gd_3Fe_5O_{12}$ system,[32] showing that the signs of the XMCD signals for Gd and Fe can be qualitatively used as an indicator of metal spin orientation.

The preliminary XMCD results for $[Fe_2^{III,II}(bpmp)(\mu\text{-}O_2CC_2H_5)_2]^{2+}$ in two different fields are shown in Figure 3. Both the absolute and relative intensities of the effects are field dependent. The XMCD spectrum for this system can be treated as the sum of individual XMCD spectra for the ferric and ferrous monomers, and it can be rationalized using an electronic spin Hamiltonian involving zero-field splittings (D), exchange interactions (J_{AB}), and Zeeman interactions.[33] In the strong 6 T field, both signals are negative, indicating that the spins are mostly parallel and that the Zeeman interaction overwhelms the zero-field splittings D and the exchange interaction J_{AB}. The observed XMCD was ~34% of the effect expected for two independent and totally oriented Fe(II) and Fe(III) ions, indicating that the temperature and field were not sufficient to achieve total spin alignment. In the weaker 1 T field, the Fe(II) XMCD becomes quite weak. There is a competition between the different terms in the spin Hamiltonian, but neglecting zero-field splittings, the antiferromagnetically coupled Fe(II) should eventually have a positive XMCD at a sufficiently weak magnetic field. Quantitative analysis requires more extensive analysis, including diagonalization of the Hamiltonian and thermal and orientation averaging.

The two iron sites in $[Fe_2(Me_3tacn)_2(\mu\text{-}OH)_3]^{2+}$ are separated by 2.50 Å,[21] the smallest distance between the two irons in the mixed-valence dimers presented here. These two high-spin irons are ferromagnetically coupled, with a $S_{total} = {}^9/_2$ ground state and with $J = 16$ cm^{-1} with $D_1 = D_2 = 2$ cm^{-1} [21] and transfer integral $B = 1320$ cm^{-1} (double exchange).[34] The spectrum, Figure 4a, somewhat resembles a high-spin Fe(II) spectrum, with both lower energy and higher energy shoulders, a satellite at the L_3-edge, and a triplet L_2 peak. However, the main L_3 and L_2 peaks are much broader than those for the divalent Fe compounds. The branching ratio of the L_3 and L_2 intensities is consistent with high-spin ground states. Simulation of a delocalized mixed-valence spectrum requires charge transfer calculations involving both d^5 and d^6 initial configurations, which will be reported separately.

The spectrum for high-spin $[Fe^{II}(tppb)_2]$ ($S = 2$), Figure 4b, resembles that for the delocalized $[Fe_2(Me_3tacn)_2(\mu\text{-}OH)_3]^{2+}$,

(31) van der Laan, G.; Thole, B. T. *Phys. Rev. B* **1991**, *43*, 13401.
(32) Rudolf, R.; Sette, F.; Tjeng, L. H.; Meigs, G.; Chen, C. T. *J. Magn. Magn. Mater.* **1992**, *109*, 109.
(33) For example, see: McCormick, J. M.; Reem, R. C.; Solomon, E. I. *J. Am. Chem. Soc.* **1991**, *113*, 9066−9079.
(34) Blondin, G.; Girerd, J. *Chem. Rev.* **1990**, *90*, 1359.

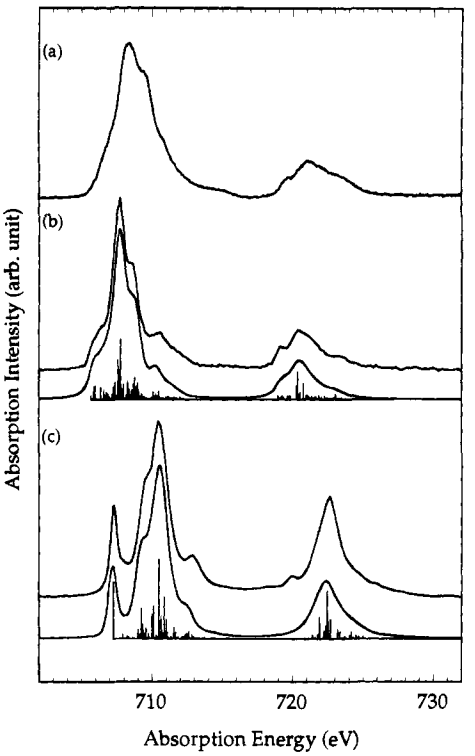

Figure 4. (a) Experimental L-edge spectrum of $[Fe^{II,III}_2(Me_3tacn)_2(\mu\text{-}OH)_3]^{2+}$. (b) Experimental L-edge spectrum (top) for $[Fe^{II}(tppb)_2]$ together with the theoretical calculation (bottom). (c) Experimental spectrum (top) for $[Fe^{III}(HB(pz)_3)_2][ClO_4]$ together with the theoretical calculation (bottom). The stick diagrams show the strengths of individual transitions before broadening.

but all of the features are sharper and at lower energy. The calculated spectrum reproduces the experimental spectrum well. Theoretical calculations show that the low-energy shoulder at the L_2-edge of the spectrum varies the most with ligand field strength. Generally, high-spin Fe(II) systems, such as $[Fe^{II}(tppb)_2]$, $[Fe^{II,II}_2(bpmp)(\mu\text{-}O_2CC_2H_5)_2]^+$, and $Fe(phen)_2(NCS)_2$ (when temperature is higher than 180 K), have similar L-edge spectra, a singlet L_3 peak with shoulders on low- and high-energy sides and a triplet L_2-edge. Low-spin Fe(II) compounds, such as $K_4[Fe(CN)_6]$ (not shown), give totally different L-edge spectra, a doublet L_3-edge with 1.7 eV separation and a sharp singlet L_2-edge with much great relative intensity.

The spectrum for low-spin $[Fe^{III}(HBpz_3)_2][ClO_4]$ is also included (Figure 4c). It is quite different from high-spin Fe(III), with a sharp peak 3.5 eV lower than the main L_3 peak, clear L_3 multiplet features, and a relatively sharp L_2 peak. The small branching ratio ($L_3/(L_3 + L_2)$ intensity) is characteristic of low-spin systems.[35] The calculation with $10Dq = 3.0$ eV agrees reasonably well with the experimental spectrum for $[Fe^{III}(HBpz_3)_2][ClO_4]$, except for missing the small feature at 720 eV and having a higher branching ratio. The calculation shows that the first L_3 peak is a singlet excitation $2p^63d^5(t_{2g}^5) \rightarrow 2p^53d^6(t_{2g}^6)$. A symmetry reduction from O_h to D_{4h} or D_{3d} does not change the spectrum signicantly, and reducing the 3d spin–orbit coupling improves the branching ratio but not the overall similarity.

To investigate the width of the spectrum for the electron-delocalized dimer, theoretical calculations were performed with different $10Dq$ values for both Fe(III) ($10Dq = 1.2$, 1.5, and 1.8 eV) and Fe(II) ($10Dq = 0.9$, 1.1, and 1.3 eV). The calculated sum spectra, even with shifted Fe(II) and Fe(III) components, were far different from the experimental spectrum for $[Fe_2(Me_3tacn)_2(\mu\text{-}OH)_3]^{2+}$. Broadness of the L_3-edge spectrum for a noninteger oxidation state of high-spin Fe(III) ($^6A_{1g}$) has also been observed in the $La_{1-x}Sr_xFeO_3$ system.[27] The undoped system has a sharp multiplet structure for the L_3-edge. Upon doping with Sr, the spectrum changes at the high-energy side of the L_3-edge and the multiplet structure diminishes, and a broadened L_3-edge peak results when x approaches 0.5. The 2p core hole absorption for the L-edge XAS measurement occurs on a short time scale of *ca.* 10^{-15} s as compared to the Mössbauer time scale of about 10^{-7} s. The L-edge XAS measurement for $[Fe^{III,II}_2(Me_3tacn)_2(\mu\text{-}OH)_3]^{2+}$ shows that, at the much shorter time scale, the electronic delocalization is the same as that determined by Mössbauer.[21]

Conclusions

Iron L-edge X-ray absorption spectroscopy has been used to study mononuclear and dinuclear iron complexes. The trapped-valence dinuclear complex spectra can be described as sums of individual spectra for isolated Fe(II) and Fe(III). Spectra for both oxidation states can be interpreted by atomic multiplet calculation with the inclusion of an adjustable ligand field. For high-spin Fe(III) and high-spin Fe(II), we found $10Dq$ around 1.5 and 1.0 eV, respectively, as expected for normal trivalent and divalent irons with oxygen or nitrogen donor ligands in octahedral symmetry. Also, the larger reduction of the Slater integrals for Fe(III) suggested a more covalent Fe site than for Fe(II).

We have shown that the sign and field strength dependence of the XMCD effect can be used to characterize the strength and type of the coupling between magnetic metal ions, using $[Fe^{III,II}_2(bpmp)(\mu\text{-}O_2CC_2H_5)_2][BPh_4]_2$ as a test case. L-edges have also been used to qualitatively distinguish the delocalized mixed-valence complex $[Fe_2(Me_3tacn)_2(\mu\text{-}OH)_3]^{2+}$. This complex exhibits a delocalized L-edge spectrum, even on the extremely short X-ray absorption time scale.

L-edge and XMCD spectroscopy together are powerful probes of mixed-valence complexes. As better detectors, magnets, cryostats, and X-ray sources are implemented, biological applications may be expected to expand.

Acknowledgment. The authors would like to thank Dr. H.-I. Lin for assistance during the synchrotron measurements. Funding for this work was obtained from the Department of Energy, Office of Health and Environmental Research, National Science Foundation (Grants DMB-91-07312 and BIR-93-17942), and the National Institutes of Health (Grant GM-44380 for S.P.C. and GM-38767 for L.Q.). The National Synchrotron Light Source is supported by the Department of Energy, Office of Basic Energy Sciences.

Supplementary Material Available: Tables of the L_3 and L_2 peak positions of the Fe L-edge absorption spectra and the parameters used for calculations (2 pages). This material is contained in many libraries on microfiche, immediately follows this article in the microfilm version of the journal, can be ordered from the ACS, and can be downloaded from the Internet; see any current masthead page for ordering information and Internet access instructions.

JA9430098

(35) Thole, B. T.; van der Laan, G. *Phys. Rev. B* **1988**, *38*, 3158.